Materials Today Bio 12 (2021) 100164

Contents lists available at ScienceDirect

Materials Today Bio

journal homepage: www.journals.elsevier.com/materials-today-bio

Photoreactive-proton-generating hyaluronidase/albumin nanoparticles-loaded PEG-hydrogel enhances antitumor efficacy and disruption of the hyaluronic acid extracellular matrix in AsPC-1 tumors

Woo Tak Lee [a], Junyeong Lee [a], Hanju Kim [a], Nguyen Thi Nguyen [a], Eun Seong Lee [b], Kyung Taek Oh [c], Han-Gon Choi [d], Yu Seok Youn [a,*]

[a] School of Pharmacy, Sungkyunkwan University, 2066 Seobu-ro, Jangan-gu, Suwon, Gyeonggi-do, 16419, Republic of Korea
[b] Department of Biotechnology and Department of Biomedical-Chemical Engineering, The Catholic University of Korea, 43 Jibong-ro, Bucheon-si, Gyeonggi-do, 14662, Republic of Korea
[c] College of Pharmacy, Chung-Ang University, 84 Heukseok-ro, Dongjak-gu, Seoul, 06974, Republic of Korea
[d] College of Pharmacy, Hanyang University, 55, Hanyangdaehak-ro, Sangnok-gu, Ansan, 15588, Republic of Korea

ARTICLE INFO

Keywords:
Photosensitive pH-jump
Hyaluronic acid
Hyaluronidase
Albumin nanoparticles
Extracellular matrix
Tumor suppression

ABSTRACT

Depletion of tumor extracellular matrix (ECM) is viewed as a promising approach to enhance the antitumor efficacy of chemotherapeutic-loaded nanoparticles. Hyaluronidase (HAase) destroys hyaluronic acid-based tumor ECM, but it is active solely at acidic pHs of around 5.0 and is much less active at physiological pH. Herein, we report the development of our novel UV-light-reactive proton-generating and hyaluronidase-loaded albumin nanoparticles (o-NBA/HAase-HSA-NPs). The method to prepare the nanoparticles was based on pH-jump chemistry using o-nitrobenzaldehyde (o-NBA) in an attempt to address the clinical limitation of HAase. When in suspension/PEG-hydrogel and irradiated with UV light, the prepared o-NBA/HAase-HSA-NPs clearly reduced the pH of the surrounding medium to as low as 5.0 by producing protons and were better able to break down HA-based tumor cell spheroids (AsPC-1) and HA-hydrogel/microgels, presumably due to the enhanced HA activity at a more optimal pH. Moreover, when formulated as an intratumor-injectable PEG hydrogel, the o-NBA/HAase-HSA-NPs displayed significantly enhanced tumor suppression when combined with intravenous paclitaxel-loaded HSA-NPs (PTX-HSA-NPs) in AsPC-1 tumor-bearing mice: The tumor volume in mice administered UV-activated o-NBA/HAase-HSA-NPs and PTX-HSA-NPs was 198.2 ± 30.0 mm^3, whereas those administered PBS or non-UV-activated o-NBA/HAase-HSA-NPs and PTX-HSA-NPs had tumor volumes of 1230.2 ± 256.2 and 295.4 ± 17.1 mm^3, respectively. These results clearly demonstrated that when administered with paclitaxel NPs, our photoreactive o-NBA/HAase-HSA-NPs were able to reduce pH and degrade HA-based ECM, and thereby significantly suppress tumor growth. Consequently, we propose our o-NBA/HAase-HSA-NPs may be a prototype for development of future nanoparticle-based HA-ECM-depleting tumor-ablating agents.

1. Introduction

The extracellular matrix (ECM) is a three-dimensional network that consists of various components such as hyaluronic acid (HA), collagen, fibronectin, and laminin [1,2]. Many solid tumors of the breast, pancreas, colon, lung and other tissues develop areas of abnormal ECM fibrosis. The increased ECM stiffness decreases blood perfusion and elevates interstitial fluid pressure (IFP) in the tumor microenvironment, and these changes reduce the uptake of chemotherapeutic agents by solid tumors and hence reduce their efficacy [3–5]. Therefore, the destruction or remodeling of the ECM has been considered an effective method to improve the delivery efficiency of antitumor agents and circumvent chemotherapeutic resistance [5,6].

Hyaluronic acid (HA), a negatively charged glycosaminoglycan (GAG) polymer of repeating N-acetyl-D-glucosamine and D-glucuronic acid disaccharide subunits, is one of the major components of tumor ECM, together with collagen [7]. Unlike the low HA density in normal tissues, HA is overexpressed in most tumors and plays a role as a significant barrier to drug diffusion [8,9]. The supportive use of the hyaluronidase (HAase) enzyme that digests tumor HA-based ECM is viewed

* Corresponding author.
E-mail address: ysyoun@skku.edu (Y.S. Youn).

https://doi.org/10.1016/j.mtbio.2021.100164
Received 27 September 2021; Received in revised form 13 November 2021; Accepted 20 November 2021
Available online 20 November 2021

as a synergistic approach to enhance the antitumor efficacy of many chemotherapeutic agents [9–12]. Intravenous or intratumor administration of HAase destroys the HA matrix and reduces the HA content in solid tumors, which enable improved drug delivery to individual cancer cells.

However, a critical limitation of clinical use of HAase is the pH-dependence of its activity. Regardless of the source and type of HAase, the digestive activity of most HAases (including commercially available) is optimal at around pH 4.5–5.5 and is abolished when the pH exceeds ~7.0 [13–15]. Human serum hyaluronidase 1 (HYAL1) is reported to be active only when the pH is less than 5.1 [16]. Thus, conventional HAases lose HA-digestive activity at both physiological pH (~7.4) and at the slightly more acidic pH of tumors (~6.6–6.8) [17,18]. In light of this clinical problem, a recombinant human HAase (rHuPH-20; HYLENEX®), which is active at both neutral and acidic pH, was developed and received US FDA approval in 2005 [19]. Alternately, the activity of the native HAase can be maintained if the local pH within the ECM is reduced to ~5.0–6.0, or the dose of HAase is considerably increased.

Previously, we developed a series of nanoparticle-albumin-bound (nab^{TM})-based formulations to suppress many solid tumors [20–23]. Furthermore, we introduced modified human serum albumin nanoparticles (HSA-NPs) embedded with macromolecules, such as tumor-necrosis-factor-related apoptosis-inducing ligand (TRAIL) and hyaluronidase [24,25]. Herein, we describe our efforts to make Abraxane™ (paclitaxel)-like HSA-NPs that generate protons in response to UV light irradiation, thus enhancing HAase activity and ECM-destruction by reducing the local pH (Fig. 1). Focusing on this purpose, we formulated injectable PEG-hydrogel containing HSA-NPs with HAase and o-nitrobenzaldehyde (o-NBA), hereafter termed o-NBA/HAase-HSA-NPs, that release HAase and induce photoreactive proton generation, respectively. The o-NBA also played a second role as a physical crosslinker to maintain the Abraxane™-like structure. The physicochemical properties of the o-NBA/HAase-HSA-NPs were investigated using relevant spectroscopic analyses. The pH-reducing ability and HA matrix-destroying performance of the o-NBA/HAase-HSA-NPs under UV light illumination were evaluated using human hepatoma HepG2 and human pancreatic adenocarcinoma AsPC-1 cell spheroids and the AsPC-1 cell-xenograft tumors *in vivo*. In addition, the antitumor effects of combining intratumoral injection of the o-NBA/HAase-HSA-NPs with intravenous paclitaxel were evaluated.

2. Materials and methods

2.1. Materials

Paclitaxel (PTX) was obtained from JW Pharmaceutical Corporation (Dangjin, South Korea). Human serum albumin, hyaluronidase (HAase; type I, 400–1,000 U/mL), and o-nitrobenzaldehyde (o-NBA) were purchased from Sigma-Aldrich (St. Louis, MO, USA). Sodium hyaluronate (HA: >100 kDa or ~8 kDa for cell spheroid) and fluorescein isothiocyanate (FITC)-labelled HA for cell spheroid (Mw ~8 kDa) were purchased from Sigma-Aldrich (St. Louis, MO, USA). The AsPC-1 and HepG2 cells were purchased from the Korean Cell Line Bank (Seoul, Korea). Polyclonal antibodies targeting hyaluronan binding protein 1 (HABP-1) were purchased from MyBioSource (San Diego, USA). Alexa-Fluor®-488-conjugated goat-anti-rabbit secondary antibodies were purchased from abcam (Cambridge, USA). Fetal bovine serum (FBS), and trypsin-EDTA and penicillin-streptomycin solutions were purchased from Capricorn (Ebsdorfergrund, Hesse, Germany) and Corning (Corning, NY, USA), respectively. Tetraglycerol-condensed ricinoleate (TGCR: SY-Glyster CR-310) was kindly provided by Sakamoto Yakuhin Kogyo Co. (Osaka, Japan). All other reagents were obtained from Sigma-Aldrich unless otherwise indicated.

2.2. Animals

The BALB/c *nu/nu* mice (male, 6 weeks old) were purchased from ORIENT BIO (Seongnam, South Korea). Animals were cared for according to the guidelines issued by the National Institutes of Health (NIH) in accordance with the care and use of laboratory animals (NIH publication 80–23, revised in 1996). Mice were grouped based on their treatment and housed and fed under a 12-h light/dark cycle (lights on at 6 a.m.). This study was approved by the Ethical Committee on Animal Experimentation at Sungkyunkwan University.

2.3. Fabrication of o-NBA/HAase-HSA-NPs and PTX-HSA-NPs

The o-NBA/HAase-HSA-NPs were fabricated as previously described using the nanoparticle albumin-bound (nab™) technique with slight modifications [22,23,25]. The nab™ technology is a well-known preparation method to encapsulate hydrophobic drugs into albumin through

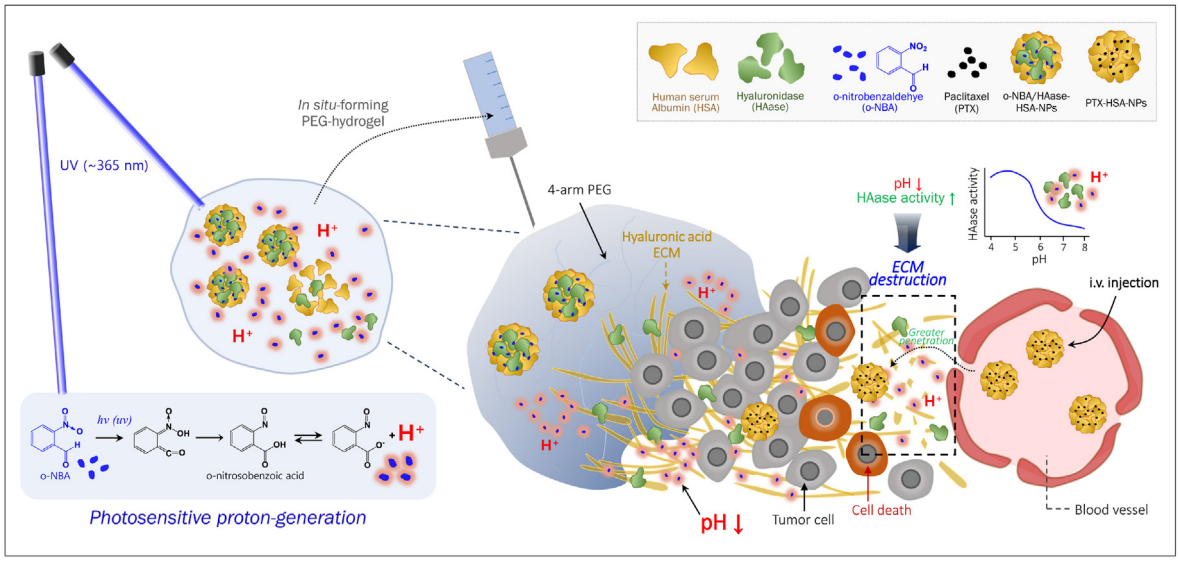

Fig. 1. Schematic illustration of antitumor therapy based upon destruction of the HA extracellular matrix due to decreased acidity using PEG-hydrogel containing UV-responsive proton-generating o-NBA/HAase-HSA-NPs in conjunction with PTX-HSA-NPs.

an emulsion-evaporation cross-link method using high-pressure homogenization without the use of Cremophor®. Briefly, aliquots of 50 mg HSA, HAase (0 and 2.5 mg) were dissolved in 5 mL deionized water (DW; 0.5 mg/mL). Aliquots (10 mg) of o-NBA were dissolved in 100 μL of a 9:1 solution of chloroform and ethanol, respectively. Solutions of each set of aqueous/organic phase were gently mixed and homogenized using a Wise Tis homogenizer HG-15D (DAIHAN Scientific Co, Seoul, South Korea) at 14,500 rpm for 3 min and then passed through a high-pressure homogenizer (EmulsiFlex-B15 device, Avestin, Ottawa, ON, Canada) for nine cycles at 20,000 psi. After removing the chloroform using a rotary evaporator at 40 °C for 15 min under reduced pressure, the resulting NPs were gently centrifuged at 6,000 rpm. The supernatant was collected and purified in Amicon® Ultra centrifugal filter units (MWCO: 100 kDa, Millipore) to remove the unbound PTX and HAase. The recovered supernatant was then freeze-dried and stored at −20 °C until needed. The PTX-HSA-NPs, which were used solely for the animal experiments, were prepared separately by using 50 mg HSA dissolved in 5 mL of deionized water (DW) and 5 mg PTX in 100 μL (50 mg/mL) of a 9:1 solution of chloroform and ethanol, respectively, according to the same procedure described above. The prepared NPs were freeze-dried and stored at −20 °C until needed.

2.4. Characterization of o-NBA/HAase-HSA-NPs and PTX-HSA-NPs

The average sizes and the zeta potentials of the o-NBA/HAase-HSA-NPs and PTX-HSA-NPs were measured using dynamic light scattering (DLS; Zetasizer Nano ZS90, Malvern Instruments, Worcestershire, UK) of a 633 nm He–Ne laser beam with a fixed 90° scattering angle. The surface morphology of the NPs was observed by transmission electron microscopy (TEM) with a model JEM-3010 (JEOL, Tokyo, Japan) and field-emission scanning electron microscopy (FE-SEM) using a JSM7000F model (JEOL, Tokyo, Japan). The physical stability of the NPs in 10 mM PBS (pH 7.4) was evaluated at room temperature by considering the maintenance of the particle size. Briefly, the particle sizes of the o-NBA/HAase-HSA-NPs and o-NBA-HSA-NPs (as redisperse forms) were monitored at every 6 h for 48 h using the DLS method described above.

2.5. Preparation of in situ gelling PEG-hydrogel for intratumoral injection of o-NBA/HAase-HSA-NPs

The o-NBA/HAase-HSA-NPs for intratumor injection were formulated using *in situ* gelling PEG-hydrogel according to the protocol described previously with modifications, considering the acidity of UV-activated o-NBA/HAase-HSA-NPs (Supplementary Data Fig. S1) [26,27]. To synthesize thiolated HSA (HSA-SH), HSA (500 mg) was dissolved in 1 mL of 100 mM PBS buffer (pH 7.5) containing 2-iminothiolane (2-IT, 12.5 mg) and then reacted by stirring for 1.5 h. The unreacted 2-IT was removed using a centricon-10 concentrator (Millipore, Bedford, MA, USA). A dry powder of 4-arm PEG_{20k}-maleimide (10 mg: NOF corporation, Tokyo, Japan) were added to 0.1 mL of o-NBA/HAase-HSA-NPs previously irradiated with 2 h UV light. The resulting solution was further mixed with 20 μl of HSA-SH (500 mg/mL), and the final mixture were then allowed to react for 90 s for gelation. The material was considered to be in a gel state if it did not flow when inverted.

2.6. Determination of PTX in paclitaxel-loaded HSA-NPs (PTX-HSA-NPs) for intravenous injection

The loading efficiency of PTX in PTX-HSA-NPs was evaluated using the following protocol. Briefly, 1 mg of the lyophilized PTX-HSA-NPs was dissolved in 0.1 mL DW. To remove bound HSA from the NPs, 0.9 mL acetonitrile (ACN) was added to the NP suspension, followed by sonication for 30 min and centrifugation at 14,500 rpm for 20 min. Subsequently, the supernatant was withdrawn for quantification. The PTX supernatant was then subjected to reverse-phase high-performance liquid chromatography (RP-HPLC) using a PLRP-S Zorbax 100 RP-18 column (150 mm × 4.6 mm, 8 μm/300 Å; Agilent Technologies, Palo Alto, CA, USA) at ambient temperature [25]. A combined gradient plus isocratic elution method was carried out at a flow rate of 1.0 mL/min using solvent A (DW) and solvent B (ACN): specifically, 0–60% B for 7 min, 60% B for 10 min, and 100% A for 4 min. Eluates were monitored at 223 nm. Three replicates of each sample were prepared and analyzed.

2.7. Preparation of fluorescent HA-hydrogel and HA-microgel as an artificial ECM

The HA-hydrogel were prepared by using previously described methods with slight modification (Supplementary Data Fig. S2) [28,29]. To synthesize FITC-tagged HA, first, 60 mg of sodium hyaluronate (HA) dissolved in DW (12 mL) was mixed with 0.1 g of 1-Ethyl-3-(3-dimethylaminopropyl)carbodiimide (EDC) and 667 mg of adipic dihydrazide (ADH). The pH of the resulting mixture was adjusted to 4.75, and the reaction was allowed to continue for 4 h and then stopped by adding NaOH (bringing the pH to 7.0). The reaction mixture was first dialyzed against a large excess of 100 mM NaCl aqueous solution for 24 h, and then against a mixed solution of ethanol and water (1:3) for 24 h, and, finally, three times against DW for 24 h, using a dialysis membrane bag (Mw 14 kDa: Spectrum Chemical, New Brunswick, NJ, USA). The resulting ADH-activated HA then was lyophilized and stored at −20 °C until needed. Second, 10 mL of FITC dissolved in anhydrous DMSO (5 mg/mL) was mixed with 50 mg of HA-ADH solution, and the reaction was allowed to continue for 12 h. The unreacted FITC was removed by dialysis in DW over 24 h, and the resulting solution corresponding to HA-ADH-FITC was freeze-dried and stored at −20 °C until needed.

The macroscopic fluorescent HA-hydrogel discs were prepared by gently mixing 1 mL of a 6:4 solution of HA (50 mg/mL) and HA-ADH-FITC (10 mg/mL) with 40 μL of divinyl sulfone (DVS: final 4% (v/v)). The gelation reaction was allowed to continue at 37 °C for 5 min in a temporary disc mold. Fluorescent hyaluronic acid hydrogel microparticles (HA-microgel) were prepared separately using a W/O emulsification method. In brief, 1 mL of a 6:4 solution of HA (30 mg/mL) and HA-ADH-FITC (10 mg/mL) was emulsified by using an overhead mechanical stirrer in 50 mL kerosene containing 1% TGCR for 30 min at 1,800 rpm. A 20 μL aliquot of divinyl sulfone (DVS: final 2% v/v to disperse phase) was added to the emulsion solution, and the resulting mixture was allowed to crosslink for 1 h for while stirred at 1,500 rpm. The hardened HA-microgel were harvested after centrifugation at 1,000 rpm, and washed two times, first with acetone and then with ethanol, under vortexing and bath sonication. The HA-microgel were then lyophilized and stored at −20 °C until needed.

2.8. Monitoring of pH-dependent degradation of HA-microgel

The HA-microgel (5 mg/mL) were mixed and incubated with 1 mL of 1 mg/mL naïve HAase in a series of phosphate buffers with pHs adjusted to 4.0, 5.0, 5.5, 6.0 and 7.4. After 2 h, the intensity of the HA-FITC fluorescence was monitored to assess the degree of degradation/release of HA microgel particles. In order to normalize the pH-dependent fluorescein emission, the pH of collected samples was set to ~10.0 using 0.1 M sodium carbonate buffer before fluorescence quantification. The fluorescence intensity was determined at excitation and emission wavelengths of 495 and 520 nm, respectively.

2.9. Degradation of HA-hydrogel and HA-microgel

To examine the HA-degrading capability of each formula group (F1~F5) (Table 1), the prepared HA-hydrogel discs (8.5 and 2.0 mm in diameter and thickness, respectively) and HA-microgel (5 mg/mL) were incubated with 1 mL of 5 mM PBS, o-NBA/HAase-HSA-NPs (each 0.5 mg/mL HAase and 10 mg/mL HSA) and o-NBA-HSA-NPs with or without the 2-h UV irradiation (2.7 mW/cm^2 at a 5-cm distance) at 37 °C. For macroscopic HA-hydrogel, at predetermined times (0, 2, 6 and 24 h), the

Table 1
Formulation and treatment groups used in this study (*in vitro* and *in vivo*).

In vitro study	Formulation groups	UV
F1	PBS (pH 7.4; 5 mM)	off
F2	o-NBA/HSA-NPs	off
F3	o-NBA/HSA-NPs	**on**
F4	o-NBA/HAase-HSA-NPs	off
F5	o-NBA/HAase-HSA-NPs	**on**
***In vivo* study**	**Treatment groups**	**UV**
G1	PBS (i.v.)	off
G2	PBS (i.v.) + naive HAase (i.t.)	off
G3	PTX-HSA-NPs	off
G4	PTX-HSA-NPs (i.v.) + o-NBA/HAase-HSA-NPs (i.t.)*	off
G5	PTX-HSA-NPs (i.v.) + o-NBA/HAase-HSA-NPs (i.t.)*	**on**

i.v.: Intravenous injection; i.t.: Intratumor injection, * PEG-hydrogel formula.

surface appearance and color of each HA-hydrogel disc was observed. The fluorescence intensity due to the HA-FITC degraded from HA-hydrogel and the resulting solution pH were measured. The mass ratio of the treated/lyophilized HA-hydrogel versus their initials was calculated to examine the degree of degradation after 48 h. Finally, the internal structural changes of HA-hydrogel (after 24 h after the treatments) were observed by field-emission scanning electron microscopy (FE-SEM) using a JSM7000F model (JEOL, Tokyo, Japan). For HA-microgel, the morphology and number of microgels within each group was monitored by using a fluorescence microscopy at 0, 2, 10 and 24 h after the treatment, and the reduced particle size (mean ± sd) of representative microgel particles remained (at lease n > at least 50–90; n = 20 for F5 at 24 h) and the OriginPro® program (OriginLab®) and the resulting solution pH until each sampling times were measured respectively. The phenol red (5 mg/mL) colors were photographed at various times depending upon the pH of the buffer and duration of UV irradiation of the o-NBA/HAase-HSA-NPs.

2.10. Cytotoxicity evaluation of o-NBA in HepG2 and AsPC-1 cells

The concentration-dependent toxicity of o-NBA was evaluated using a conventional 3-(4,5-dimethylthiazol-2-yl)-2,5-diphenyltetrazolium bromide (MTT) assay. Briefly, HepG2 cells were seeded into 96-well plates at a density of 1×10^6 cells/well in DMEM media containing 10% (v/v) fetal bovine serum and 1% penicillin/streptomycin in a 5% CO_2, 95% RH incubator at 37 °C. Following 24 h incubation, the cells were incubated with 0–3000 μg/mL of o-NBA and irradiated with a UV laser (365 nm) for 2 h or received no irradiation, and then further incubated for 24 h. The cell viability was assessed by using an MTT assay.

2.11. Degradation of spheroids made of HepG2 or AsPC-1 cells

The HepG2 and AsPC-1 cells were cultured in DMEM and RPMI media, respectively, containing 10% (v/v) fetal bovine serum and 1% penicillin/streptomycin in a 5% CO_2, 95% RH incubator at 37 °C. The HepG2 and AsPC-1 cells (1,000 and 2,000 cells per well, respectively) were seeded into v-bottom cell plates (Shimadzu, Kyoto, Japan) designed to induce the formation of 3D multicellular spheroids, and HA-fluorescein (200 μg/mL; Sigma Aldrich, St. Louis, MO, USA) was added to only the HepG2 cells. The HepG2 and AsPC-1 cell spheroids were then allowed become established over three days before further experiments. To investigate HA degradation in the ECM as well as in the spheroids, tumor spheroids were incubated with o-NBA/HAase-HSA-NPs and o-NBA-HSA-NPs (each 0.5 mg/mL HAase and 10 mg/mL HSA) prepared with or without prior 2-h UV irradiation. The degradation pattern and morphology of the respective spheroids were monitored using optical microscopy. The HA-FITC-embedded cell spheroids were visualized separately using confocal laser scanning microscopy (CLSM; LSM510, Carl Zeiss Meditec AG, Jena, Germany).

2.12. Monitoring of hyaluronic acid expression in AsPC-1 cell spheroids

The expression or secretion of hyaluronic acid in AsPC-1 cell spheroids was confirmed using indirect immunofluorescence. In brief, the spheroids were fixed with 4% formaldehyde for 10 min and allowed to incubate for 5 min with 0.1% Triton x-100. The resulting cell spheroids were incubated with the blocking solution (1% BSA, 22.52 mg/mL glycine in PBST [PBS containing 0.1% Tween 20]) for 1 h, and then the anti-HA-binding-protein (HABP)-1 primary antibodies (diluted 1:100 in 1% BSA in PBST) were added and the mixtures incubated overnight in a humidified chamber at room temperature. The spheroids were washed three times in PBS and incubated with both Alexa-Fluor®-488-conjugated secondary antibodies (diluted 1:100 in 1% BSA in PBST) were added and the mixtures incubated at room temperature in the dark for 4 h. The secondary antibody solution was removed, and the spheroids were washed three times with PBS. After incubation with DAPI (to stain DNA) for 2 h and rinsing with PBS, the spheroids were finally visualized using CLSM.

2.13. In vivo imaging of o-NBA/Cy5.5.-HAase-HSA-NPs and PTX-Cy5.5-HSA-NPs

The *in situ* gelling PEG-hydrogel loaded with o-NBA/Cy5.5-HAase-HSA-NPs (100 μl) were directly injected to the tumor of the AsPC-1 cell-xenografted mice. Separately, an aliquot (100 μl) of PTX-Cy5.5-HSA-NPs was injected via the tail vein of AsPC-1 cell-bearing mice. The HAase and HSA had been modified with Cy5.5-NHS (GE Healthcare, Chicago, USA) and dialyzed to remove unreacted Cy5.5 before preparation of HSA nanoparticles. The Cy5.5-fluorescence signals from the tumors were visualized at predetermined times using the FOBI *in vivo* imaging system (NeoScience, Suwon, Korea).

2.14. In vivo antitumor efficacy of animal study

The AsPC-1 cells (100 μL of 7×10^6 cells/mL) were injected subcutaneously into the dorsal flanks of the mice. When the volume of the tumors reached ~150 mm^3, the mice were randomly divided into five groups (G1~G5) as follows (Table 1): (I) PBS (i.v.); (II) PBS + naive HAase (intratumor; 500 μg/0.1 mL); (III) PTX-HSA-NPs (200 μg PTX/mouse); (IV) PTX-HSA-NPs (200 μg PTX/mouse) + o-NBA/HAase-HSA-NPs (500 μg HAase and no UV); (V) PTX-HSA-NPs (200 μg PTX/mouse) + o-NBA/HAase-HSA-NPs (500 μg HAase with UV). Either PBS or PTX-HSA-NPs was injected into the tail vein 12 h after the intratumor injection of naive HAase or o-NBA/HAase-HSA-NPs for groups II, IV and V. This dosing plan was carried out on Days 0, 8, and 16. The tumor size was measured every day, and the volume (V) was calculated as follows: $V = 0.5 \times A \times B^2$, where A is the longest diameter (mm), and B is the shortest diameter (mm). On Day 24, the mice were sacrificed, and their tumors were excised and photographed. The excised tumors were fixed in a formalin solution.

Hematoxylin and eosin (H&E), Alcian Blue, HABP-1 and DAPI staining, and *in vivo* TUNEL analyses were carried out by Genoss (Suwon, Korea).

2.15. Data analyses

All data are presented as the mean ± standard deviation (SD). Significant differences were determined using Student's t-tests. For all experiments, P values < 0.01 were considered statistically significant.

3. Results

3.1. Preparation and characterization of o-NBA/HAase-HSA-NPs and PTX-HSA-NPs

The o-NBA/HAase-HSA-NPs were prepared at 2.5 mg HAase and 10

mg o-NBA using a high-pressure homogenizer based on the nab™ technique. In this formula, o-NBA was used as a physical crosslinker to associate the albumin molecules like the paclitaxel role of Abraxane®. Pure o-NBA was found to be freely soluble (~150 mg/mL) when added to a 9:1 solution of chloroform and ethanol, and this high solubility was utilized in our Nab™-based method. Consistent with previously reported results [25], HAase was used to destroy hyaluronic acid in the ECM and became incorporated into the albumin nanoparticle structure despite the high molecular size of HAase. Our previous result indicated that the conformation structure of HSA after the preparation was changed negligibly in spite of the HSA exposure to organic solvents and high-pressure [25].

As shown in the MALDI-TOF (matrix-assisted laser desorption/ionization time-of-flight) mass spectra (Supplementary Data Fig. S3-1–4), the molecular mass of HSA obtained from o-NBA/HAase-HSA-NPs was slightly higher than that of naïve HSA (66636.8 and 66522.9 *m/z*, respectively), whereas the molecular masses of HAases from each sample showed no difference (15571.8 and 15572.6 *m/z*, respectively). Also, the quantity of o-NBA extracted from o-NBA/HAase-HSA-NPs was compared to that of the o-NBA from the formula mixture (quickly harvested without nanoparticle preparation steps) using the reversed-phase HPLC. The recovery percent (%) (before vs. after the nanoparticle preparation steps) of o-NBA was found to be ~99.0 ± 1.2% (Supplementary Data Fig. S3-5–6).

The prepared o-NBA/HAase-HSA-NPs and o-NBA-HSA-NPs were found to be ~170.7 and ~152.2 nm in diameter, respectively (Fig. 2A). Additionally, the particle size of PTX-HSA-NPs, which were used for the intravenous injection in the antitumor efficacy animal study, were ~146.2 nm in diameter. The zeta potentials of all the NPs were similar, being approximately −21 mV primarily due to the negative charge of albumin (Fig. 2B). The o-NBA was quite soluble in the 9:1 solution of chloroform/ethanol but poorly soluble in water. The o-NBA/HAase-HSA-NPs samples dispersed well, and their colloidal dispersions after preparation and reconstitution appeared to be clear, indicating good nanoparticle stability (Fig. 2C and Supplementary Data Fig. S4). The TEM and FE-SEM images revealed that these nanoparticles were spherical and highly homogenous in size (Fig. 2D and Supplementary Data Fig. S5). Additionally, the particle size of o-NBA/HAase-HSA-NPs were monitored while being held at room temperature for 48 h to evaluate their short-term stability. As shown in Fig. 2E, the particle sizes of the o-NBA/HAase-HSA-NPs were relatively stable over this period. Additionally, > 90% of PTX was known to be released from PTX-HSA-NPs over 24 h after the incubation in our previous articles [24,25], which was useful for determining dosing interval for *in vivo* efficacy study.

3.2. Evaluation of pH-dependent degradation of fluorescent HA-microgel by HAase

HA-microgel with green fluorescence were prepared using the w/o emulsification method and using HA and FITC-labelled HA. As shown in Fig. 3A and B-inset, the prepared HA-microgel were spherical and homogenous (84. 2 ± 5.8 μm) (Supplementary Data Fig. S6) in diameter at a fully swollen state and displayed strong green fluorescence under CSLM. The morphology and particle-number-based density of fluorescent HA-microgel incubated with HAase were monitored at different pHs. As

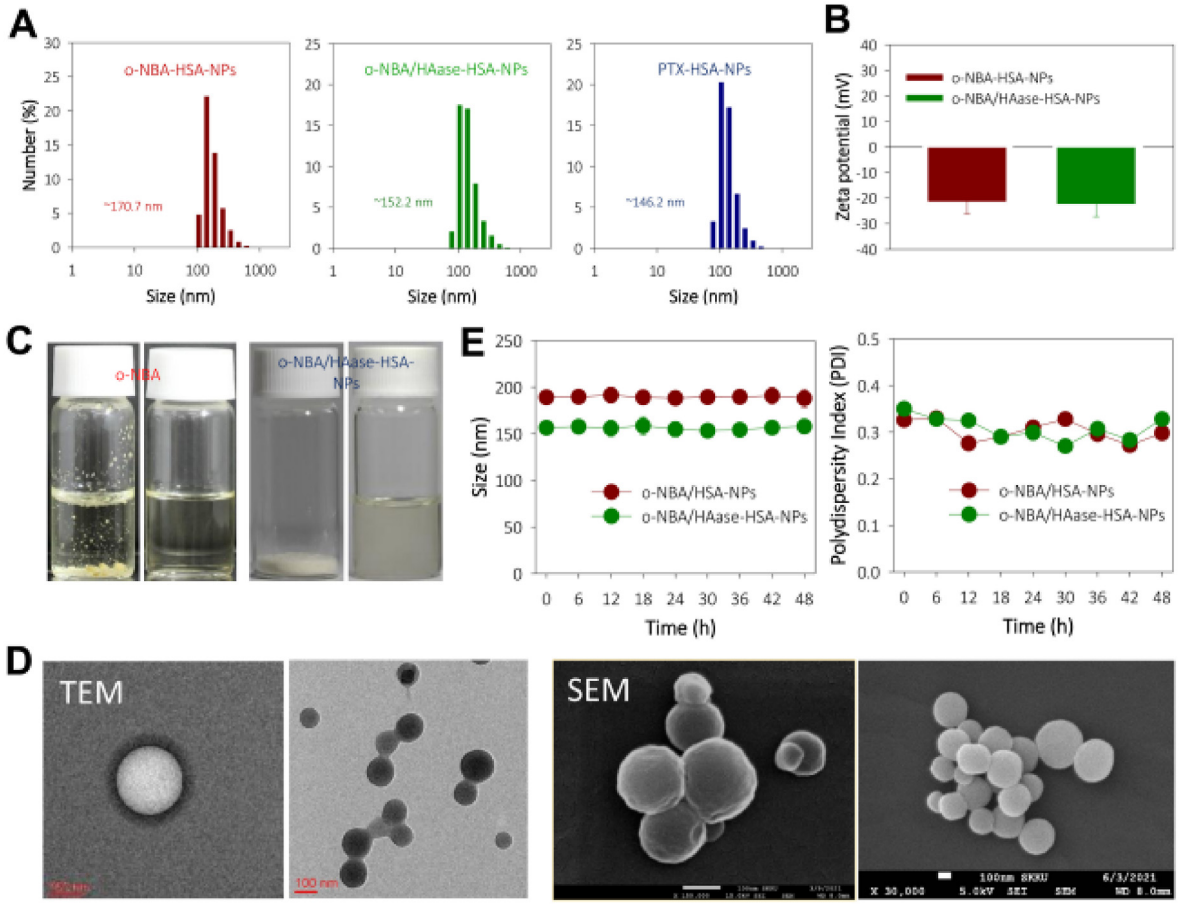

Fig. 2. (A) Histograms of particle sizes of o-NBA-HSA-NPs, o-NBA/HAase-HSA-NPs and PTX-HSA-NPs (B) Zeta potentials of o-NBA-HSA-NPs and o-NBA/HAase-HSA-NPs. (C) Photographs of o-NBA in DW (left) and a 9:1 solution of chloroform and ethanol (right) and the lyophilized powder (left) and dispersed solution (right) of o-NBA/HAase-HSA-NPs. (D) Transmission electron microscopy (TEM; left) and field-emission scanning electron microscopy (FE-SEM) images of o-NBA/HAase-HSA-NPs. (E) Physical stability of o-NBA-HSA-NPs and o-NBA/HAase-HSA-NPs based on size changes (left) and polydispersity index (PDI; right).

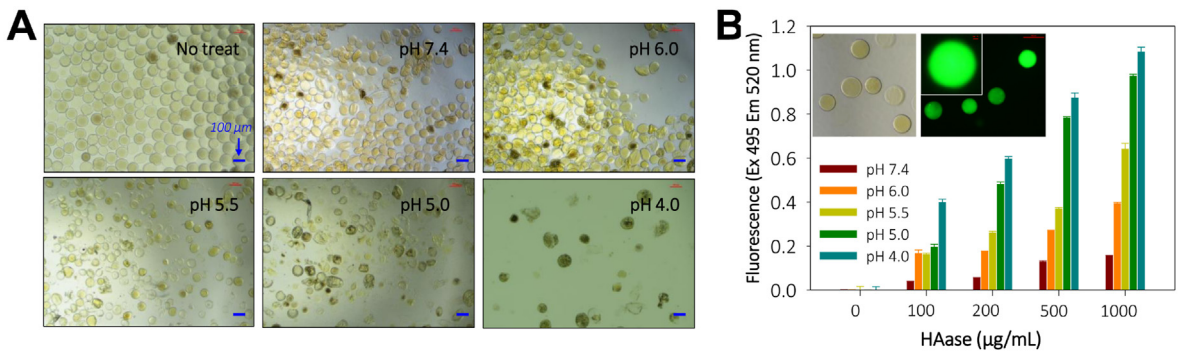

Fig. 3. Monitoring of pH-dependent hyaluronidase activity based on FITC-HA microgel degradation. (A) Optical microscopic morphology of HA-microgel (5 mg/mL) incubated with naïve HAase (1 mg/mL) at a pH of 4.0, 5.0, 5.5, 6.0 or 7.4. (B) The relative fluorescence of the supernatants from the degraded FITC-HA-microgel. Inset: enlarged HA microgel as viewed in optical microscopic (left) and confocal microscopic images (right).

shown in Fig. 3A, the HA-microgel incubated with HAase at pH 7.4 or 6.0 were negligibly degraded without significant reduction of particle numbers, but the spherical structure was significantly damaged. However, reducing the pH from 6.0 to 4.0 clearly reduced the number of microgel particles, primarily due to HA degradation: the particle morphology was deformed, and a considerable fraction of microgel particles were removed at pH 4.0 or 5.0. The pH-dependent degradation of HA-microgel by HAase was also confirmed by the increased fluorescence intensity: increasing HAase concentration and decreasing the pH of the media increased the FITC-based fluorescence intensity of supernatant, which was derived from the degraded fragments of HA-FITC of the microgels (Fig. 3B). Consequently, HAase was found to be much more active at low pH (4.0–5.0) than at a neutral pH of 7.4.

3.3. Degradation of HA-hydrogel by o-NBA/HAase-HSA-NPs with UV light

The HA-degrading activity of o-NBA/HAase-HSA-NPs was evaluated in macroscopic HA-hydrogel in the different treatment groups: F1 for 5 mM PBS (pH 7.4); F2 and F3 for o-NBA-HSA-NPs without or with UV light, respectively; F4 and F5 for o-NBA/HAase-HSA-NPs without or with UV light, respectively. As shown in Fig. 4A, the HA-hydrogel did show no significant changes in terms of shape and color (F1). However, the supernatants recovered from HA-hydrogel treated with o-NBA-HSA-NPs or o-NBA/HAase-HSA-NPs turned opaque due to degradation of the FITC-HA structure and was more obvious in the F3 and F5 o-NBA plus UV light groups. Based on the fluorescence intensity, the degradation of HA-hydrogel treated with o-NBA-HSA-NPs without HAase (F2/F3) was

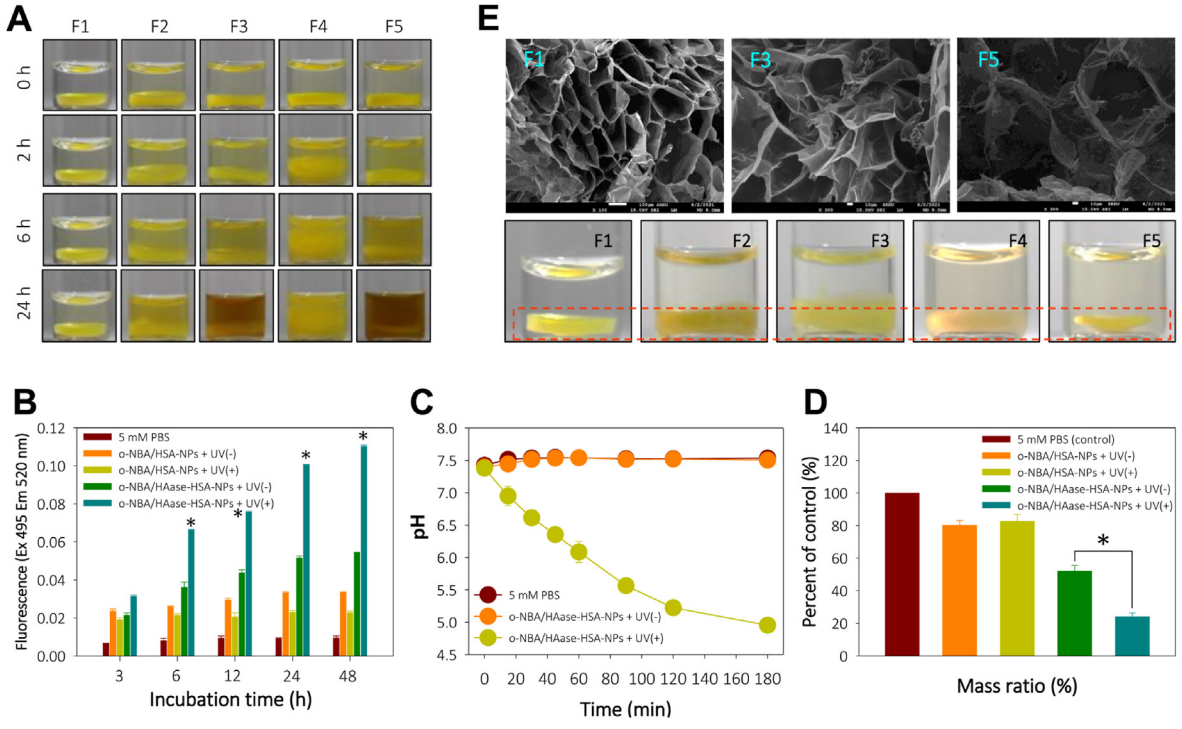

Fig. 4. HA matrix-breaking activity of o-NBA/HAase-HSA-NPs exposed to UV light (2.7 mW/cm^2 at 5 cm distance). The HA-hydrogel disc was approximately 8.5 and 2.0 mm in diameter and thickness, respectively. An 1 mL aliquot of 5 mM PBS (pH 7.4) was used as a media. (A) Photographs of macroscopic HA-hydrogel breakdown after 24 h incubation with different formulations after 2-h UV irradiation of the NPS: F1 = 5 mM PBS; F2 = o-NBA/HSA-NPs and no UV; F3 = o-NBA/HSA-NPs with UV; F4 = o-NBA/HAase-HSA-NPs and no UV; F5 = o-NBA/HAase-HSA-NPs with UV. (B) The relative fluorescence of the supernatants from the degraded FITC-HA-hydrogel incubated with F1 to F5 formulas. (C) Monitoring of pH change induced by o-NBA/HAase-HSA-NPs with or without UV light. (D) Mass ratios of F1 to F5 hydrogels versus their initial weight. *P < 0.001 over no-UV group (F4). (E) SEM images of F1, F3 and F5 after 24 h-incubation (top) and photographs of PBS-washed HA-hydrogels (F1~F5) after 24 h-incubation.

insignificant, whereas those treated with o-NBA/HAase-HSA-NPs (F4/F5) was significant. The greatest degradation was in the hydrogel treated with o-NBA/HAase-HSA-NPs plus 2-h UV light irradiation (F5), based on morphology and fluorescence intensity at Days 1 and 2, respectively (Fig. 4B). In particular, the pH of F5 hydrogels treated with o-NBA/HAase-HSA-NPs and UV light decreased rapidly to ~5.0 within 3 h, whereas the pH change of F4 without UV irradiation was negligible (Fig. 4C). Consequently, the mean mass of the F5 hydrogels was 24.2 ± 3.4% of the original mass at 48 h as a result of HA degradation, which was much lower than that of F4 hydrogels (52.2 ± 3.4%; Fig. 4D), showing the greatest degradation at F5 (Fig. 4E, bottom). Finally, the SEM imaging indicated the internal network structure of F5 hydrogels was somewhat different from F1 and F3 hydrogels (control PBS and no hyaluronidase), suggestive of greater HA degradation (Fig. 4E).

3.4. Degradation of HA-microgel by o-NBA/HAase-HSA-NPs with UV light

The HA-degrading activity of o-NBA/HAase-HSA-NPs was evaluated in HA-microgel subjected to the same treatments as for the HA macroscopic hydrogels. The shape, morphology and particle size changes of microgels in F1, F2 and F3 were not significantly altered by any treatment. However, the particle-number-based density of microgels in the F4 and F5 groups decreased greatly, and their particles become much smaller than those of the F1 microgel group (PBS control; Fig. 5A). In particular, the particles of the F5 microgel group disappeared very quickly even at 2 h after irradiation of o-NBA/HAase-HSA-NPs with UV light. After treatment, the apparent particle size of the F5 group microgels was found to be much smaller (~25 μm) than their initial size (~85 μm) (Fig. 5B; and Supplementary Data Fig. S6). The pH of the medium rapidly decreased to ~5.0 within 2 h due to the activation of o-NBA by UV irradiation (Fig. 5D), and the reduction in the pH drop was clearly indicated by the change in color of the phenol red indicator (Fig. 5C).

3.5. Cytotoxicity evaluation of o-NBA at HepG2 and AsPC-1 cells

The cytotoxicity of o-NBA was assessed in HepG2 and AsPC-1 cells prior to completing the spheroid degradation experiment. As shown in Fig. 6A and B, the HepG2 and AsPC-1 cell viabilities declined gradually as the o-NBA concentration was increased to 3 mg/mL. Approximately 20% of both HepG2 and AsPC-1 cells were killed at the highest concentration of o-NBA (1 mg/mL) tested, but UV irradiation did not affect the cytotoxicity results.

3.6. Degradation of tumor spheroids by o-NBA/HAase-HSA-NPs

The spheroids were formed from two cancer cells, hepatoblastoma HepG2 and pancreatic AsPC-1; these cell lines are known to develop significant density of hyaluronic acid and ECM at the relevant tumors. As shown in Fig. 7A, the morphology and shape of HepG2 spheroids treated with 1% medium and the F4 formula (o-NBA/HAase-HSA-NPs without UV light) were not significantly altered, but the size of spheroids treated with F4 appeared smaller than prior to treatment. The HepG2 spheroids treated with the F5 formula (o-NBA/HAase-HSA-NPs with UV light) began to shrink and degrade after 2 h and were notably deformed after 6 h incubation (after the 2 h UV irradiation), showing cellular clusters separated from the initial spheroid. In another set of HepG2 spheroids, the surface degradation of the spheroids seemed more obvious, and the spheroids were broken into clusters of cells at 12 h (Fig. 7A, bottom). The exogenous FITC-labelled HA incorporated into HepG2 cell spheroids was visualized by CLSM, and it seemed to be embedded homogenously in the spheroids (Fig. 7B).

As shown in Fig. 8A, the hyaluronic acid was well developed or secreted at the surface of each cell of the AsPC-1 spheroids because the fluorescence of HABP-1/Alexa-488 was presented. This finding indicated that the AsPC-1 cell spheroids could mimic some of the features of HA ECM-containing tumor tissues *in vivo*. The degradation of spheroids by o-NBA/HAase-HSA-NPs plus UV light was much more evident in the AsPC-1 cell spheroids (Fig. 8B). In treatment groups F1 to F4, significant degradation was not observed, except small punctures or cracks in the center region of the spheroids (F4). However, the AsPC-1 spheroids were unambiguously broken into smaller cell clusters after treatment with the F5 formula, likely due to optimized HAase activity at the low pH induced by the proton production of the o-NBA activated. by UV.

3.7. PEG-hydrogel formulation containing o-NBA/HAase-HSA-NPs

On the basis of the thiol-maleimide reaction, the PEG-hydrogel containing o-NBA/HAase-HSA-NPs formed rapidly within ~90 s after simple mixing. Although the thiol-maleimide reaction proceeds more rapidly at

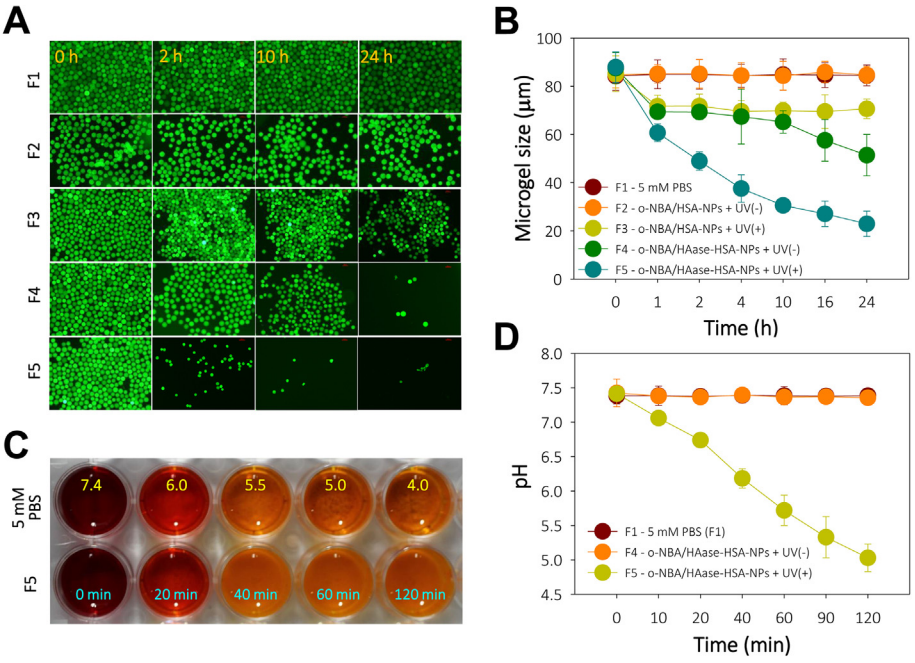

Fig. 5. HA matrix-breaking activity of o-NBA/HAase-HSA-NPs exposed to UV light (2 h, 2.7 mW/cm^2 at 5 cm distance). (A) Optical images of HA-microgel incubated with different formulas over 24 h: 5 mM PBS (F1); o-NBA/HSA-NPs + UV(−) (F2); o-NBA/HSA-NPs + UV(+) (F3); o-NBA/HAase-HSA-NPs + UV(−) (F4); o-NBA/HAase-HSA-NPs + UV(+) (F5). (B) Monitoring of microgel size change at each formula of F1~F5. (C) Monitoring of color change of phenol red at different pHs or o-NBA/HAase-HSA-NPs with UV light. (D) Monitoring of pH change induced by o-NBA/HAase-HSA-NPs with or without UV light exposure. (For interpretation of the references to color in this figure legend, the reader is referred to the Web version of this article.)

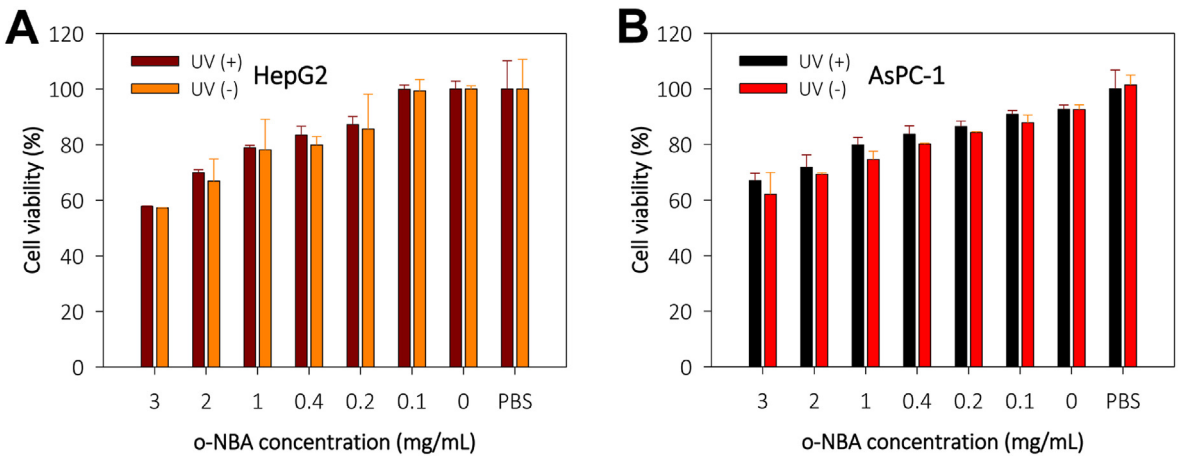

Fig. 6. Cytotoxic effects of o-NBA at various concentrations with or without UV light in HepG2 and AsPC-1 cells as measured using the MTT assay.

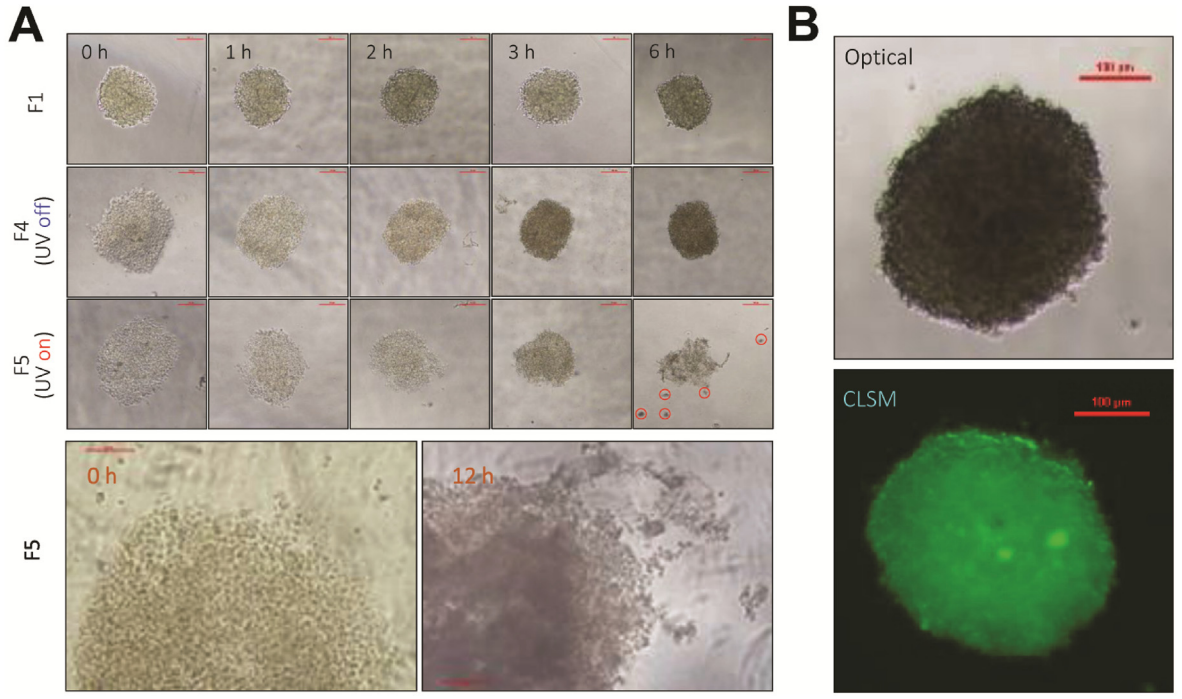

Fig. 7. (A) Monitoring of morphology of HepG2 cell spheroids incubated with 5 mM PBS (pH 7.4) and o-NBA/HAase-HSA-NPs (with or without UV exposure). Enlarged surface analysis of HepG2 cell spheroids incubated with o-NBA/HAase-HSA-NPs (with UV). (B) Optical and CLSM images of HepG2 cell spheroids embedded with FITC-conjugated low molecular weight HA (Mw ~8 kDa).

neutral pH, and the pH of UV-activated o-NBA/HAase-HSA-NPs was reduced, the resulting PEG-hydrogel displayed adequate gel properties, such that the resulting *in situ* gel did not flow or drip even when turned upside-down (Fig. 9A).

3.8. In vivo tumor localization and decay of PTX-Cy5.5-HSA-NPs and PEG-hydrogel with loaded o-NBA/Cy5.5-HAase-HSA-NPs in AsPC-1-tumor-bearing mice

After intravenous injection of PTX- Cy5.5-HSA-NPs and intratumor injection of o-NBA/Cy5.5-HAase-HSA-NPs, the NPs were monitored in AsPC-1 tumor-bearing mice. The PEG-hydrogel with loaded o-NBA/Cy5.5-HAase-HSA-NPs were diffusely distributed within the tumors, and their NIR-fluorescence signal gradually decreased and then faded out 72 h after intratumor injection (Fig. 9B). The PTX-Cy5.5-HSA-NPs accumulated gradually and peaked at 12 h in the mouse tumors and appeared to have been eliminated within 72 h after i.v. injection.

3.9. Antitumor effect of combined therapy with PTX-HSA-NPs and PEG-hydrogel with loaded o-NBA/HAase-HSA-NPs in AsPC-1-tumor-bearing mice

The antitumor effects of combined therapy with PTX-HSA-NPs and PEG-hydrogel with loaded o-NBA/HAase-HSA-NPs were evaluated in AsPC-1-tumor-bearing mice, as shown in Fig. 9C. The tumor volumes for each group of mice were measured over 14 days after treatment (Fig. 10A): the final tumor volumes for the G1 to G5 groups were 1230.2 ± 256.2, 676.3 ± 78.8, 402.2 ± 24.6, 295.4 ± 17.1, and 198.2 ± 30.0 mm^3, respectively. A single intratumor injection of naïve HAase reduced the tumor volume as compared with the PBS control group. Intravenous injection of PTX-HSA-NPs (200 μg PTX/mouse on Days 0, 8, and 16) suppressed tumor growth, but the tumors nonetheless grew gradually

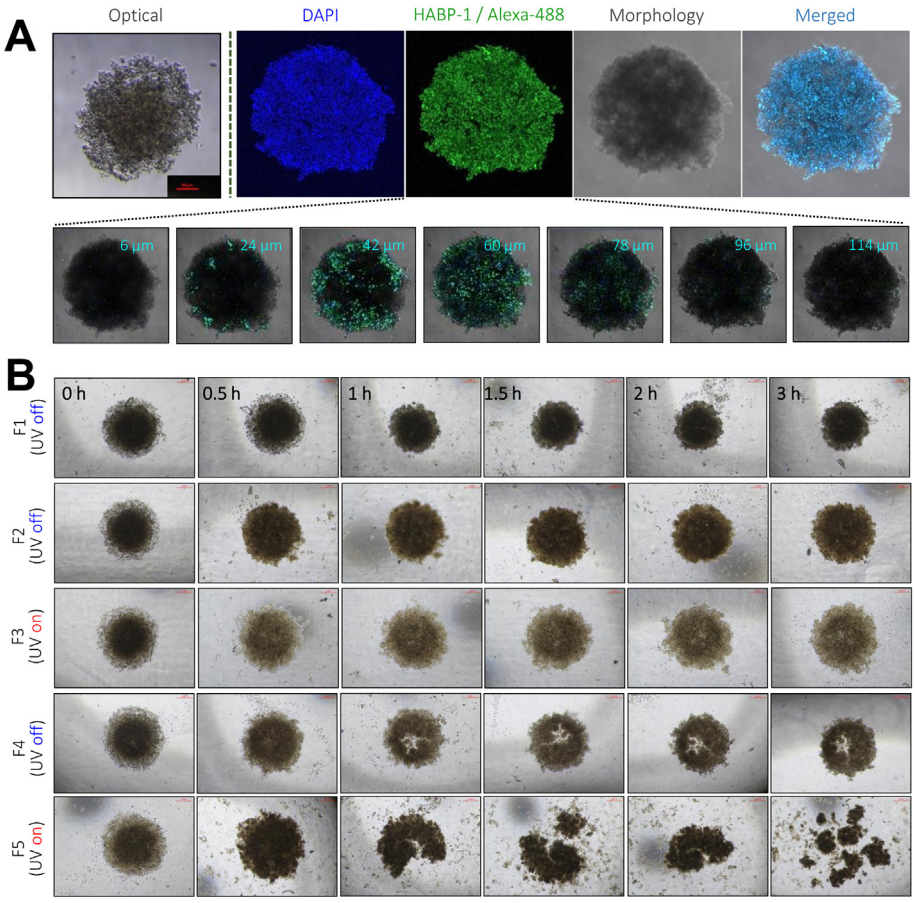

Fig. 8. (A) Optical and CLSM fluorescence images of hyaluronic acid development in AsPC-1 cell spheroids using HABP-1/Alexa-488 dye staining (bottom: z-stack images of nine 18-μm slices obtained). (B) Monitoring of morphology of AsPC-1 cell spheroids incubated with the F1 to F5 formulations over 3 h.

over 24 days. Remarkably, tumor growth in mice treated with a combination of PTX-HSA-NPs and o-NBA/HAase-HSA-NPs plus UV light was significantly suppressed, and tumor size was 7-fold and 5-fold smaller than in mice administered the PBS control and PTX-HSA-NPs-only group, respectively (Fig. 10B, C and 10D). Particularly, the tumor volumes of mice treated with a combination of PTX-HSA-NPs and o-NBA/HAase-HSA-NPs plus UV light (G5) was significantly smaller than that without UV light (G4) ($P < 0.008$ over G4 at 20–24 days) (Fig. 10B), despite small difference of their photo images. The weight of the mice in the four treatment groups was maintained without significant change over 14 days, indicating that all mice were well cared for without deleterious effects during the entire therapy period (Fig. 10E).

Tumor suppression was also assessed in the G1 to G5 treatment groups 24 days after initiation of treatment based on cell density and color intensity after various histologic staining procedures. As shown in Fig. 11, the photographic images of H&E− and Alcian blue-stained tumor sections from control groups displayed typical tumor overgrowth patterns, whereas the H&E image of sectioned tumors from mice of the G4 and G5 groups showed much weaker staining, indicating significant removal of compacted tumor tissues due to cell death. Especially, the Alcian blue staining displayed the destruction of HA in the ECM of the relevant tumors. This pattern was similar also at the HABP-1-stained tumors, but the difference of color intensity was not greatly significant (G4 and G5 vs. G3). The TUNEL images showed that the tumors of the G4 and G5 groups were partially or entirely killed due to increased apoptosis, showing clear fluorescence images of G4 and G5.

4. Discussion

Therapeutic nanoparticle-treated tumors are not effectively cured because they are protected by the ECM that hampers tumor vascular function and delivery of antitumor agents [30]. Hyaluronic acid is considered one of the most significant components of the ECM that limits antitumor therapy because it plays a role as a barrier to deep tumor penetration of nanoparticles and is present in many types of tumors [30]. Since many other ECM components are present and mingled with tumor cells in clinical cancers, the single HA-target therapy can be restricted. Nevertheless, the HAase-aided antitumor therapy has been viewed as one of the best ways of improving antitumor chemotherapy because the destruction/degradation of tumor HA is clinically effective [7,10,12,31]. Intratumor HAase injection (~1500 U) has been shown to reduce the interstitial fluid pressure (IFP) and to increase tumor uptake of liposomal doxorubicin in an OHS xenograft model [31]. Enzymatic depletion of HA using a PEGylated version of PH20 (PEG-rHuPH20; 1.5–15 mg/kg) reduced the tumor IFP and induced improved antitumor responses in a PC3 xenograft model [7]. These approaches were well performed to enhance nanoparticle delivery and antitumor efficacy [10,12]. In this respect, we focused on improving the capability of HA-destruction/reduction of our formulation in HA-hydrogel, spheroids and xenograft AsPC-1 tumors, on the basis of optimizing the HAase activity by pH jump.

Many enzymes exhibit obvious pH-dependent catalytic actions and are therefore maximally active at an optimal pH; for some enzymes,

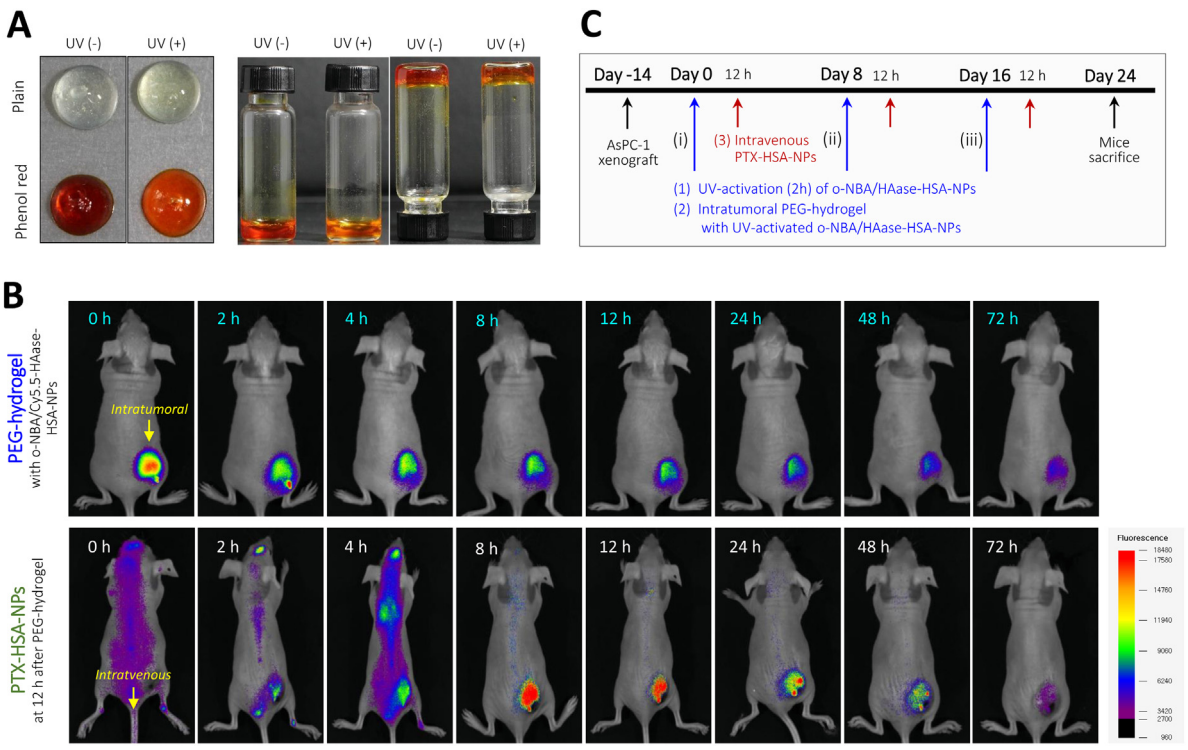

Fig. 9. (A) Photographs of *in situ* gelling of the PEG-hydrogel formula o-NBA/HAase-HSA-NPs and phenol red with or without UV light. (B) *In vivo* visualization of AsPC-1-tumor bearing mouse treated with PEG-hydrogel loaded with o-NBA/Cy5.5-HAase-HSA-NPs (intratumor injection) and PTX- Cy5.5-HSA-NPs (tail vein injection). (C) Antitumor therapy plan for combination of intravenous PTX-HSA-NPs (200 μg PTX/mouse) and intratumoral o-NBA/HAase-HSA-NPs (500 μg HAase and UV). (For interpretation of the references to colour in this figure legend, the reader is referred to the Web version of this article.)

maximal activity occurs at acidic pHs. For example, acid phosphatase produces full hydrolytic activity toward the substrate 6-chloro-8-fluoro-4-methylumbelliferone phosphate (CF-MUP) at pH 5.5, whereas it has only 3% activity at a slightly basic pH of 8.0 [32]. As noted above, HAase has maximal activity at a pH of ~5.0 and progressively loses its activity as the pH increases up to 7.4. Similar pH-dependent activity was also demonstrated in our experiment using HA-microgel as a substrate: naïve HAase showed the greatest HA-degrading activity (increased fluorescence in the supernatant) at around pH 4–5 (Fig. 3) [13–15]. We suspected that reduction of the pH at HA-containing tumor sites helped to augment the activity of the injected HAase. In this regard, the photo-switching of enzyme activity by a laser-induced pH jump is viewed as a unique method to facilitate the use of enzymes [32]. As a photoreactive proton source for a pH jump, *ortho*-nitrobenzaldehyde (o-NBA) has been widely used because it is strongly and rapidly activated by light energy: nitrosobenzoic acid is formed extremely fast (in 7 ps) after o-NBA irradiation with UV light (266 nm) [33,34]. More specifically, o-NBA undergoes intramolecular excited-state hydrogen transfer (ESHT) upon UV irradiation to form 2-nitrosobenzoic acid through a bicyclic benzisoxazolidine intermediate, which is able to produce a proton and thus reduces the pH of the local environment [32,35,36]. As shown in Figs. 4 and 5, o-NBA embedded into albumin nanoparticles was found to be highly responsive to UV light and significantly reduced the pH of the medium to ~5.0 in a relatively short time period (2 h). The HA-hydrogel and HA-microgel were significantly degraded by augmented HAase activity aided by proton generation of UV-activated o-NBA in a pH-dependent manner. Moreover, the extracellular pH of tumors is known to be acidic (pH 6.5–6.8) due to aerobic glycolysis (Warburg effect), which is lower than that of blood pH (7.4) [37]. However, altering the pH in a macroscopic drug delivery system, such as a hydrogel, or in a specific site of body is a huge challenge, contrary to the easily penetrating stimuli (e.g., heat, light and magnetic field etc.) [38].

Albumin is a useful pharmaceutical excipient for parenteral formulations and is also used as a natural targeting carrier for chemotherapeutics [39,40]. Moreover, it provides inner molecular space to bind many hydrophobic drugs, and this binding improves apparent drug solubility and extends the half-life of drugs [41,42]. Likewise, albumin plays a role as a kind of matrix for hydrophobic drugs before their release-out. Regarding the Abraxane® (Celgene Corp.) product, paclitaxel is attached to hydrophobic crevice of albumin and physically crosslinks albumin molecules. At this base, o-NBA was almost insoluble in water and but was highly soluble in a chloroform and ethanol mixture (Fig. 2). Solubilization enabled the formation of albumin nanoparticles with sufficient o-NBA incorporated within them to enable a pH jump. In essence, albumin nanoparticles were used as a reservoir matrix, and o-NBA played a role as a physical crosslinker to assemble albumin nanoparticles. Albumin nanoparticles are known to be targeted to solid tumors through tumor extravasation and gp60-mediated transcytosis [43,44]. Recently, nab™-paclitaxel (Abraxane®) was used in combination with gemcitabine and the PEGylated version of PH20 (PEG-r-HuPH20) in a Phase II metastatic pancreatic cancer trial aimed at removing HA-based ECM from tumor regions and thereby creating a novel effective anti-pancreatic tumor therapy. This clinical study has shown an increased survival in treated patients as compared with control patients [45]. We have assessed the use of the nab™-technique to incorporate large proteins (i.e., TRAIL [~66 kDa] and HAase [60 kDa]) into albumin nanoparticles [24,25] and optimized the formulation for incorporation of HAase (0.5 mg) into o-NBA/HAase-HSA-NPs.

Particularly, the amine-aldehyde reaction between HSA and o-NBA was one of important issues because this covalent reaction might reduce free o-NBA in the formula and thus ruin the pH-jump. Considering the precision limit (~0.1%) of MALDI-TOF MS, the mass difference between HSAs before and after the preparation (~114) appeared to be a bit significant and due to the o-NBA (151.12 Da) conjugation to HSA. Consequently, 0.76 o-NBA molecule was estimated to be covalently bound to 1 HSA molecule (presumably any amine of 59 amines in an HSA).

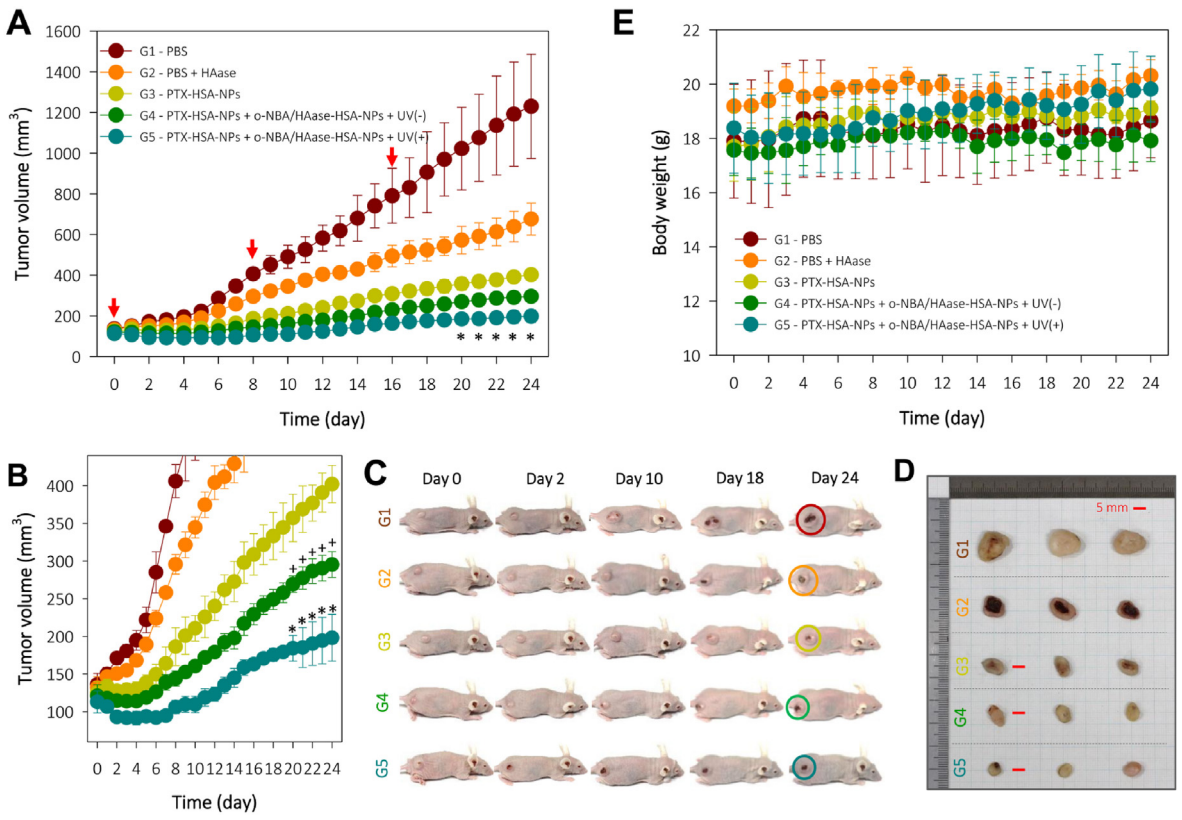

Fig. 10. *In vivo* antitumor efficacy of PEG-hydrogel containing UV-responsive o-NBA/HAase-HSA-NPs in conjunction with PTX-HSA-NPs in five mouse treatment groups: (I) PBS (i.v.); (II) PBS + naive HAase (intratumor; 500 μg/0.1 mL); (III) PTX-HSA-NPs (200 μg PTX/mouse); (IV) PTX-HSA-NPs (200 μg PTX/mouse) + o-NBA/HAase-HSA-NPs (500 μg HAase and UV(−)); (V) PTX-HSA-NPs (200 μg PTX/mouse) + o-NBA/HAase-HSA-NPs (500 μg HAase and UV(+)). (A) Tumor volumes in each group over 24 days. (B) Focused tumor volume profiles of G3, G4 and G5 over 24 days ($^{+}P < 0.009$ over G3 and $^{*}P < 0.008$ over G4). (C) Representative photographs of AsPC-1 tumor-bearing mice at the indicated days after treatment. (D) Photographs of tumors excised from each treatment group. (E) Body weight change of AsPC-1 tumor-bearing mice in the different treatment groups over 24 days post-treatment.

However, considering the fed molar ratio of HSA and o-NBA (1: 88), approximately 0.86% of whole o-NBA appeared to be bound to HSA, and hence ~99% of o-NBA remain intact as a free form. This calculated value was consistent with the recovery percent (%) (before vs. after the nanoparticle preparation steps; ~99.0 ± 1.2%), which was quantitated by RP-HPLC (Supplementary Data Fig. S3-5–6). As a result, ~99% of o-NBA fed was able to participate in the UV-activated pH-jump reaction. These two molecules are present at separate organic and aqueous phases, respectively, when being homogenized, and solid-state o-NBA are embedded into HSA molecule after evaporation. Therefore, the amine-aldehyde substitution reaction between HSA and o-NBA, otherwise undermines the pH-jump, seemed to be negligible (<1%) because both molecules had less chance to interact during the preparation.

Consequently, the prepared o-NBA/HAase-HSA-NPs were apparently able to generate protons in response to UV light and release HAase, which resulted in accelerated breakdown of HA matrix *in vitro* and *in vivo*. This coordinated HA-degrading activity of o-NBA/HAase-HSA-NPs was clearly demonstrated in HA-hydrogel/microgel and in HepG2/AsPC-1 cell spheroids. Additionally, the HA-degrading activity of o-NBA/HAase-HSA-NPs appeared to be more obvious in pancreatic AsPC-1 cell spheroids that develops more HA in the EMC than in hepatocarcinoma HepG2 spheroids (Figs. 7 and 8). In more than 90% of pancreatic tumors HA formation is significant, especially in ductal/mucinous adenocarcinomas [30]. Although HepG2 secretes HA [46], the HA amount seemed a bit lower for the degradation study in our study. Therefore, extra HA was added to the HepG2 spheroids in our experiments in order to better mimic the *in vivo* tumor ECM environment. Nonetheless, the HepG2 spheroid seemed resistant to the degradation by HAase even at a low pH of ~5.0 (Fig. 6). However, o-NBA/HAase-HSA-NPs displayed much clear HA ECM-degrading activity in AsPC-1 cell spheroid, which presumably contributed to improving the *in vivo* antitumor of nanoparticle-based chemotherapeutics. Subsequently, pancreatic AsPC-1 cells were chosen for the xenograft tumor model based on degree of HA development and sensitivity to HAase. Separately, a single cellular spheroid using either HepG2 or AsPC-1 was used in this study, but recently multicellular spheroid is viewed as an ideal model mimicking actual tumors because these tumor cell aggregates have complex dynamic cell–cell/cell–matrix interactions [47]. Therefore, the evaluation of o-NBA/HAase-HSA-NPs system in the multicellular spheroid system would be more predictive for its performance in clinical setting.

PTX-HSA-NPs were injected intravenously to deliver paclitaxel to the xenograft tumors, as shown in the success of Abraxane® [39]. On the contrary, o-NBA/HAase-HSA-NPs were directly injected into the tumors so as to ensure effective pH-jump and activate the HAase because the UV light irradiation should be focused on the higher level of o-NBA/HAase-HSA-NPs entrapped by the PEG-hydrogel. Likewise, hyaluronidase or collagenase is usually injected into the tumors to accelerate the ECM breakdown. In general, quantitative analyses have demonstrated that HA staining of tumors is not greatly significant in xenografted tumor models [10], presumably because both degraded HA fragments (low Mw: 1–2 kDa) as well as intact high molecular weight HA might be stained [4]. Thus, the extent of HA-ECM destruction is difficult to demonstrate *in vivo*. For this and clarifying the antitumor effect of each group, the dosing plan was achieved three time at 0, 8 and 16 days. Presumably due to the repeated dosing, the histologies of Alcian blue and HABP-1 in G5 seemed slight better, albeit not great, than those in G3 and G4 in the context of HA depletion. In AsPC-1 cell xenografted mice, UV-activated HA-degrading activity of o-NBA/HAase-HSA-NPs was indirectly demonstrated

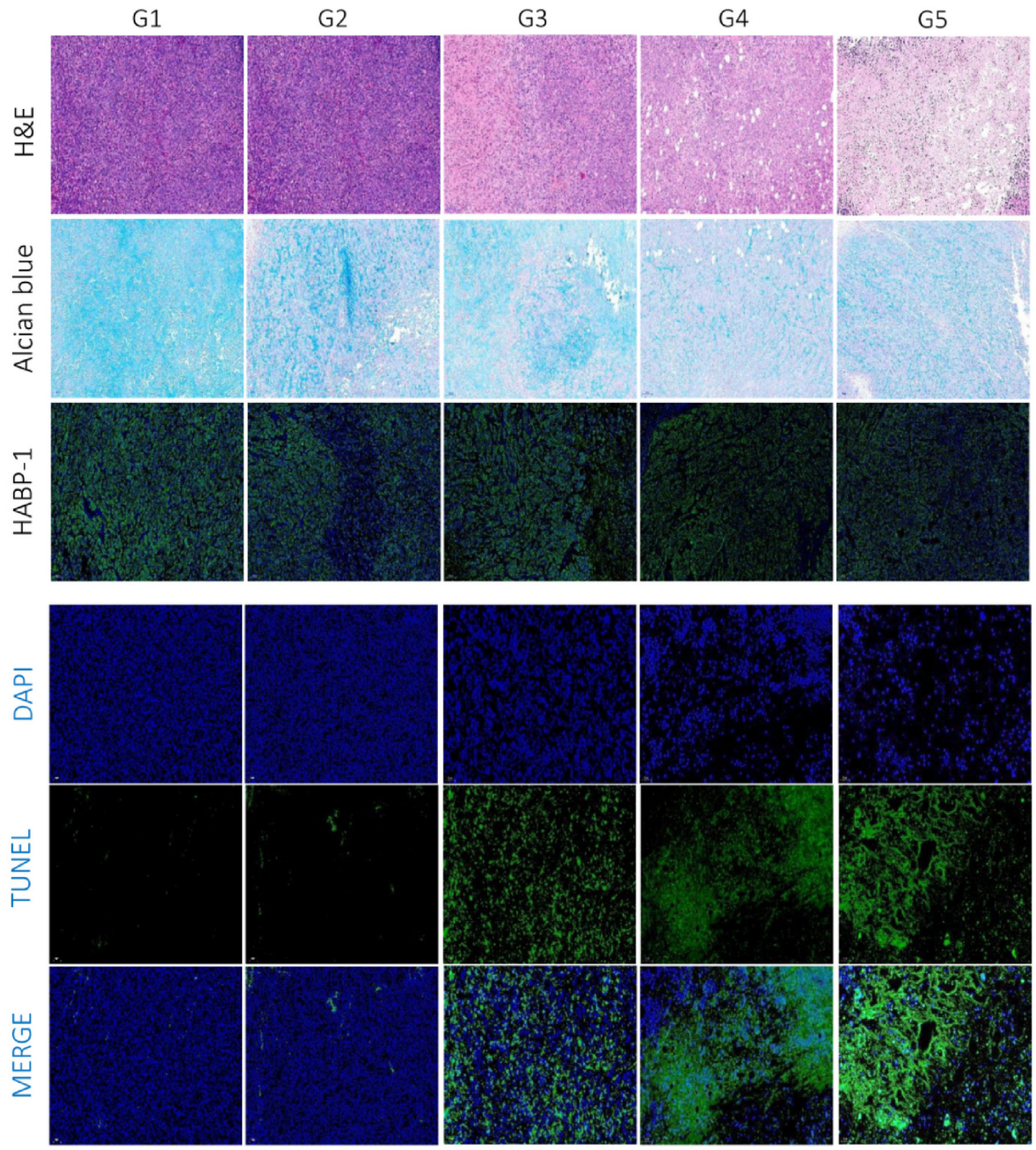

Fig. 11. (A) Microscopic images showing H&E, Alcian blue, HABP-1, DAPI and TUNEL staining of tumor slices from mice of each treatment group of G1∼G5. blue and HA-specific staining of tumor slices from mice of each treatment group. (For interpretation of the references to colour in this figure legend, the reader is referred to the Web version of this article.)

by increased tumor suppression when administered in conjunction with intravenous injection of paclitaxel-loaded albumin nanoparticles (200 μg/mice). For intratumor injection, o-NBA/HAase-HSA-NPs were formulated as an *in situ* injectable PEG-hydrogel as in our previous studies (Fig. 9) [26,27,48]. This hydrogel prototype showed good performance for sustained release of HAase *in vivo* because the 4-arm PEG was a large crosslinker and the thiol-maleimide reaction did not involve conjugation with HAase.

Consequently, the tumors of mice treated with o-NBA/HAase-HSA-NPs with UV light and PTX-HSA-NPs were clearly significantly reduced in volume compared with those of all other groups. The tumor size reduction in the HAase-only group without PTX injection was likely due to degradation of the HA matrix that facilitates tumor growth. Although the reductions in tumor size in the UV and no-UV groups as compared with the control group were very small, the differences were statistically significant ($P < 0.009$), which indicated that our objective of (i) UV-activated proton generation and (ii) optimization of HAase activity had been successfully attained. Additionally, a better way of sending or generating UV light around in deep tumor sites is maneuvered to maximize the ECM-breaking activity for *in vivo* clinical performance because UV light penetrate into skin or tumor tissues less than deep red near infrared (NIR: 650–900 nm) on account of its short wavelength [49]. In this context, future investigations of o-NBA/HAase-HSA-NPs as UV light-emitting upconverting nanoparticles responding to NIR light can be considered a next step in development of the HAase-based platform.

5. Conclusion

In summary, we fabricated a prototype of UV light-reactive proton-generating hyaluronidase/albumin nanoparticles having enhanced hyaluronic acid-degrading activity based on a pH-jump induced by o-nitrobenzaldehyde. The UV light-activated o-NBA/HAase-HSA-NPs were found to reduce the local pH to ~5.0 and exhibited clear HA-degrading capability in ECM-mimicking models of HA-hydrogel/microgel and AsPC-1 tumor cell spheroids. Furthermore, the *in situ* intratumor-injectable PEG-hydrogel formula of o-NBA/HAase-HSA-NPs displayed significantly enhanced tumor suppression when administered with intravenous paclitaxel-loaded HSA-NPs. Overall, our results showed photoreactive o-NBA/HAase-HSA-NPs was effective in degrading HA-based ECM and suppressing tumor growth. Therefore, we believe that the o-NBA/HAase-HSA-NPs formula should be considered a prototypical HA-ECM depleting tumor-ablation agent.

Credit author statement

Woo Tak Lee: Data curation, Methodology, Writing- Original draft, Conceptualization Junyeong Lee: Data curation, Methodology Hanju Kim: Data curation Nguyen Thi Nguyen: Investigation, Visualization Eun Seong Lee: Supervision Kyung Taek Oh: Supervision Han-Gon Choi: Supervision Yu Seok Youn: Conceptualization, Writing- Original draft, Writing- Reviewing and Editing.

Declaration of competing interest

The authors declare that they have no competing financial interests or personal relationships that could have appeared to influence the work reported in this paper.

Acknowledgments

This work was supported by a National Research Foundation of Korea (NRF) grant funded by the Korean government (MSIT; No. NRF-2019R1A2C2085292 and No. NRF-2019R1A5A2027340).

References

[1] J.A. Eble, S. Niland, The extracellular matrix in tumor progression and metastasis, Clin. Exp. Metastasis 36 (2019) 171–198.
[2] C.J. Whatcott, H. Han, R.G. Posner, G. Hostetter, D.D. Von Hoff, Targeting the Tumor Microenvironment in Cancer: Why Hyaluronidase Deserves a Second Look, AACR, 2011.
[3] P.A. Netti, D.A. Berk, M.A. Swartz, A.J. Grodzinsky, R.K. Jain, Role of extracellular matrix assembly in interstitial transport in solid tumors, Cancer Res. 60 (2000) 2497–2503.
[4] A. Dolor, F.C. Szoka Jr., Digesting a path forward: the utility of collagenase tumor treatment for improved drug delivery, Mol. Pharm. 15 (2018) 2069–2083.
[5] Y.S. Youn, Y.H. Bae, Perspectives on the past, present, and future of cancer nanomedicine, Adv. Drug Deliv. Rev. 130 (2018) 3–11.
[6] U. Prabhakar, H. Maeda, R.K. Jain, E.M. Sevick-Muraca, W. Zamboni, O.C. Farokhzad, S.T. Barry, A. Gabizon, P. Grodzinski, D.C. Blakey, Challenges and Key Considerations of the Enhanced Permeability and Retention Effect for Nanomedicine Drug Delivery in Oncology, AACR, 2013.
[7] C.B. Thompson, H.M. Shepard, P.M. O'Connor, S. Kadhim, P. Jiang, R.J. Osgood, L.H. Bookbinder, X. Li, B.J. Sugarman, R.J. Connor, Enzymatic depletion of tumor hyaluronan induces antitumor responses in preclinical animal models, Mol. Cancer Therapeut. 9 (2010) 3052–3064.
[8] B.P. Toole, Hyaluronate and hyaluronidase in morphogenesis and differentiation, Am. Zool. 13 (1973) 1061–1065.
[9] P. Scodeller, Hyaluronidase and other extracellular matrix degrading enzymes for cancer therapy: new uses and nano-formulations, J. Carcinog. Mutagen. 5 (2014) 2–6.
[10] H. Zhou, Z. Fan, J. Deng, P.K. Lemons, D.C. Arhontoulis, W.B. Bowne, H. Cheng, Hyaluronidase embedded in nanocarrier PEG shell for enhanced tumor penetration and highly efficient antitumor efficacy, Nano Lett. 16 (2016) 3268–3277.
[11] S.R. Hingorani, W.P. Harris, J.T. Beck, B.A. Berdov, S.A. Wagner, E.M. Pshevlotsky, S.A. Tjulandin, O.A. Gladkov, R.F. Holcombe, R. Korn, Phase Ib study of PEGylated recombinant human hyaluronidase and gemcitabine in patients with advanced pancreatic cancer, Clin. Cancer Res. 22 (2016) 2848–2854.
[12] H. Gong, Y. Chao, J. Xiang, X. Han, G. Song, L. Feng, J. Liu, G. Yang, Q. Chen, Z. Liu, Hyaluronidase to enhance nanoparticle-based photodynamic tumor therapy, Nano Lett. 16 (2016) 2512–2521.
[13] H. Lenormand, B. Deschrevel, J.-C. Vincent, pH effects on the hyaluronan hydrolysis catalysed by hyaluronidase in the presence of proteins: Part I. Dual aspect of the pH-dependence, Matrix Biol. 29 (2010) 330–337.
[14] V. Volfova, P. Volf, The salivary hyaluronidase and apyrase of the sand fly Sergentomyia schwetzi (Diptera, Psychodidae), Insect Biochem. Mol. Biol. 102 (2018) 67–74.
[15] T. Honda, T. Kaneiwa, S. Mizumoto, K. Sugahara, S. Yamada, Hyaluronidases have strong hydrolytic activity toward chondroitin 4-sulfate comparable to that for hyaluronan, Biomolecules 2 (2012) 549–563.
[16] S. Reitinger, J. Müllegger, B. Greiderer, J.E. Nielsen, G. Lepperdinger, Designed human serum hyaluronidase 1 variant, HYAL1ΔL, exhibits activity up to pH 5.9, J. Biol. Chem. 284 (2009) 19173–19177.
[17] G. Helmlinger, F. Yuan, M. Dellian, R.K. Jain, Interstitial pH and pO_2 gradients in solid tumors in vivo: high-resolution measurements reveal a lack of correlation, Nat. Med. 3 (1997) 177–182.
[18] R. Van Sluis, Z.M. Bhujwalla, N. Raghunand, P. Ballesteros, J. Alvarez, S. Cerdán, J.P. Galons, R.J. Gillies, In vivo imaging of extracellular pH using 1H MRSI, Magn. Reson. Med. 41 (1999) 743–750.
[19] G.N. Cherr, S.A. Meyers, A.I. Yudin, C.A. VandeVoort, D.G. Myles, P. Primakoff, J.W. Overstreet, The PH-20 protein in cynomolgus macaque spermatozoa: identification of two different forms exhibiting hyaluronidase activity, Dev. Biol. 175 (1996) 142–153.
[20] B. Kim, B. Seo, S. Park, C. Lee, J.O. Kim, K.T. Oh, E.S. Lee, H.-G. Choi, Y.S. Youn, Albumin nanoparticles with synergistic antitumor efficacy against metastatic lung cancers, Colloids Surf. B Biointerfaces 158 (2017) 157–166.
[21] H.J. Byeon, S. Lee, S.Y. Min, E.S. Lee, B.S. Shin, H.-G. Choi, Y.S. Youn, Doxorubicin-loaded nanoparticles consisted of cationic-and mannose-modified-albumins for dual-targeting in brain tumors, J. Contr. Release 225 (2016) 301–313.
[22] P.T.T. Phuong, S. Lee, C. Lee, B. Seo, S. Park, K.T. Oh, E.S. Lee, H.-G. Choi, B.S. Shin, Y.S. Youn, Beta-carotene-bound albumin nanoparticles modified with chlorin e6 for breast tumor ablation based on photodynamic therapy, Colloids Surf. B Biointerfaces 171 (2018) 123–133.
[23] P.T.T. Pham, X.T. Le, H. Kim, H.K. Kim, E.S. Lee, K.T. Oh, H.-G. Choi, Y.S. Youn, Indocyanine green and curcumin Co-loaded nano-fireball-like albumin nanoparticles based on near-infrared-induced hyperthermia for tumor ablation, Int. J. Nanomed. 15 (2020) 6469.
[24] S.Y. Min, H.J. Byeon, C. Lee, J. Seo, E.S. Lee, B.S. Shin, H.-G. Choi, K.C. Lee, Y.S. Youn, Facile one-pot formulation of TRAIL-embedded paclitaxel-bound albumin nanoparticles for the treatment of pancreatic cancer, Int. J. Pharm. 494 (2015) 506–515.
[25] S.S. Kim, H.K. Kim, H. Kim, W.T. Lee, E.S. Lee, K.T. Oh, H.-G. Choi, Y.S. Youn, Hyperthermal paclitaxel-bound albumin nanoparticles co-loaded with indocyanine green and hyaluronidase for treating pancreatic cancers, Arch Pharm. Res. (Seoul) 44 (2021) 182–193.
[26] I. Kim, J.S. Choi, S. Lee, H.J. Byeon, E.S. Lee, B.S. Shin, H.-G. Choi, K.C. Lee, Y.S. Youn, In situ facile-forming PEG cross-linked albumin hydrogels loaded with an apoptotic TRAIL protein, J. Contr. Release 214 (2015) 30–39.
[27] C. Lee, K. Lim, S.S. Kim, E.S. Lee, K.T. Oh, H.-G. Choi, Y.S. Youn, Near infrared light-responsive heat-emitting hemoglobin hydrogels for photothermal cancer therapy, Colloids Surf. B Biointerfaces 176 (2019) 156–166.
[28] M. Ge, J. Sun, M. Chen, J. Tian, H. Yin, J. Yin, A hyaluronic acid fluorescent hydrogel based on fluorescence resonance energy transfer for sensitive detection of hyaluronidase, Anal. Bioanal. Chem. 412 (2020) 1915–1923.
[29] E.J. Oh, S.W. Kang, B.S. Kim, G. Jiang, I.H. Cho, S.K. Hahn, Control of the molecular degradation of hyaluronic acid hydrogels for tissue augmentation, J. Biomed. Mater. Res. 86 (2008) 685–693.
[30] M.A. Jacobetz, D.S. Chan, A. Neesse, T.E. Bapiro, N. Cook, K.K. Frese, C. Feig, T. Nakagawa, M.E. Caldwell, H.I. Zecchini, Hyaluronan impairs vascular function and drug delivery in a mouse model of pancreatic cancer, Gut 62 (2013) 112–120.
[31] L. Eikenes, M. Tari, I. Tufto, Ø.S. Bruland, C. de Lange Davies, Hyaluronidase induces a transcapillary pressure gradient and improves the distribution and uptake of liposomal doxorubicin (Caelyx™) in human osteosarcoma xenografts, Br. J. Cancer 93 (2005) 81–88.
[32] S. Kohse, A. Neubauer, A. Pazidis, S. Lochbrunner, U. Kragl, Photoswitching of enzyme activity by laser-induced pH-jump, J. Am. Chem. Soc. 135 (2013) 9407–9411.
[33] M.L. Donten, P. Hamm, pH-Jump overshooting, J. Phys. Chem. Lett. 2 (2011) 1607–1611.
[34] S. Laimgruber, W.J. Schreier, T. Schrader, F. Koller, W. Zinth, P. Gilch, The photochemistry of o-nitrobenzaldehyde as seen by femtosecond vibrational spectroscopy, Angew Chem. Int. Ed. Engl. 44 (2005) 7901–7904.
[35] H.W. Choi, J. Kim, J. Kim, Y. Kim, H.B. Song, J.H. Kim, K. Kim, W.J. Kim, Light-induced acid generation on a gatekeeper for smart nitric oxide delivery, ACS Nano 10 (2016) 4199–4208.
[36] A. Migani, V. Leyva, F. Feixas, T. Schmierer, P. Gilch, I. Corral, L. González, L. Blancafort, Ultrafast irreversible phototautomerization of o-nitrobenzaldehyde, Chem. Commun. 47 (2011) 6383–6385.
[37] Y. Wang, K. Zhou, G. Huang, C. Hensley, X. Huang, X. Ma, T. Zhao, B.D. Sumer, R.J. DeBerardinis, J. Gao, A nanoparticle-based strategy for the imaging of a broad range of tumours by nonlinear amplification of microenvironment signals, Nat. Mater. 13 (2014) 204–212.

[38] P. Techawanitchai, M. Ebara, N. Idota, T. Aoyagi, Light-induced spatial control of pH-jump reaction at smart gel interface, Colloids Surf. B Biointerfaces 99 (2012) 53–59.
[39] F. Kratz, Albumin as a drug carrier: design of prodrugs, drug conjugates and nanoparticles, J. Contr. Release 132 (2008) 171–183.
[40] E.S. Lee, Y.S. Youn, Albumin-based potential drugs: focus on half-life extension and nanoparticle preparation, J Pharm Investig 46 (2016) 305–315.
[41] S. Bae, K. Ma, T.H. Kim, E.S. Lee, K.T. Oh, E.-S. Park, K.C. Lee, Y.S. Youn, Doxorubicin-loaded human serum albumin nanoparticles surface-modified with TNF-related apoptosis-inducing ligand and transferrin for targeting multiple tumor types, Biomaterials 33 (2012) 1536–1546.
[42] S.H. Choi, H.J. Byeon, J.S. Choi, L. Thao, I. Kim, E.S. Lee, B.S. Shin, K.C. Lee, Y.S. Youn, Inhalable self-assembled albumin nanoparticles for treating drug-resistant lung cancer, J. Contr. Release 197 (2015) 199–207.
[43] A.O. Elzoghby, W.M. Samy, N.A. Elgindy, Albumin-based nanoparticles as potential controlled release drug delivery systems, J. Contr. Release 157 (2012) 168–182.
[44] F. Kratz, A clinical update of using albumin as a drug vehicle–A commentary, J. Contr. Release 190 (2014) 331–336.
[45] S. Hingorani, A. Bullock, T. Seery, L. Zheng, D. Sigal, P. Ritch, F. Braiteh, M. Zalupski, N. Bahary, W. Harris, PEGPH20 improves pfs in patients with metastatic pancreatic ductal adenocarcinoma: a randomized phase 2 study in combination with nab-paclitaxel/gemcitabine, Ann. Oncol. 28 (2017) 137–138.
[46] E. Chen, S. Han, B. Song, L. Xu, H. Yuan, M. Liang, Y. Sun, Mechanism investigation of hyaluronidase-combined multistage nanoparticles for solid tumor penetration and antitumor effect, Int. J. Nanomed. 15 (2020) 6311.
[47] X. Cui, Y. Hartanto, H. Zhang, Advances in multicellular spheroids formation, J. R. Soc. Interface 14 (2017) 20160877.
[48] H.J. Byeon, S.H. Choi, J.S. Choi, I. Kim, B.S. Shin, E.S. Lee, E.-S. Park, K.C. Lee, Y.S. Youn, Four-arm PEG cross-linked hyaluronic acid hydrogels containing PEGylated apoptotic TRAIL protein for treating pancreatic cancer, Acta Biomater. 10 (2014) 142–150.
[49] P. Avci, A. Gupta, M. Sadasivam, D. Vecchio, Z. Pam, N. Pam, M.R. Hamblin, Low-level laser (light) therapy (LLLT) in skin: stimulating, healing, restoring, Seminars in cutaneous medicine and surgery, Semin. Cutan. Med. Surg. 32 (2013) 41–52.